# Organic/Inorganic Hybrid Nanochannels Based on Polypyrrole-Embedded Alumina Nanopore Arrays: pH- and Light-Modulated Ion Transport

*Qianqian Zhang, Zhaoyue Liu,* Kefeng Wang, and Jin Zhai**

**Inspired by the asymmetric structure and responsive ion transport in biological ion channels, organic/inorganic hybrid artificial nanochannels exhibiting pH-modulated ion rectification and light-regulated ion flux have been constructed by introducing conductive polymer into porous nanochannels. The hybrid nanochannels are achieved by partially modifying alumina ($Al_2O_3$) nanopore arrays with polypyrrole (PPy) layer using electrochemical polymerization, which results in an asymmetric component distribution. The protonation and deprotonation of $Al_2O_3$ and PPy upon pH variation break the surface charge continuity, which contributes to the pH-tunable ion rectification. The ionic current rectification ratio is affected substantially by the pH value of electrolyte and the pore size of nanochannels. Furthermore, the holes (positive charges) in PPy layer induced by the cooperative effect of light and protons are used to regulate the ionic flux through the nanochannels, which results in a light-responsive ion current. The magnitude of responsive ionic current could be amplified by optimizing this cooperation. This new type of stimuli-responsive PPy/$Al_2O_3$ hybrid nanochannels features advantages of unique optical and electric properties from conducting PPy and high mechanical performance from porous $Al_2O_3$ membrane, which provide a platform for creating smart nanochannels system.**

## 1. Introduction

Biological ion channels that intelligently regulate ion transport through cell membranes in response to environmental multi-stimuli provide the inspiration to create biomimetic responsive solid-state artificial nanochannels.[1] The responsive artificial nanochannels are typically built by chemical modification of nanochannels using stimuli-responsive molecules or employing stimuli-responsive materials as the body component.[2] Compared with biological ion channels, their abiotic analogues feature several advantages such as controllable geometry and size, robust mechanical strength, and excellent chemical stability, which may boost the development of bioinspired smart nanodevices for potential applications.[3] In order to make artificial nanochannels possess more similar qualities to their biological counterparts, endowing artificial nanochannels to respond to multi-stimuli is of great importance. To date, a series of ionic gates responding to pH and temperature was built by introducing two kinds of functional molecules or multi-responsive molecules into single nanochannels.[4] Light- and pH-responsive molecules were also used to functionalize the single nanochannels to realize multi-stimuli-response function.[5] Recently, pH- and voltage-gated single nanochannel was obtained by modifying polymer nanopore with responsive DNA oligomers.[6] However, these stimuli-responsive artificial nanochannels are usually based on organic single nanochannel, whose complex fabrication procedures,[7] low chemical stability and mechanical strength restrict their promising applications. Therefore, developing new system of artificial nanochannels responding to multiple stimuli is still of great significance.

Polypyrrole (PPy), as one of the most widely investigated conducting polymers with extending $\pi$-conjugated electron systems, offers potential for use in the field of photoelectric devices.[8] Because of its strong absorption in the visible spectral range and high mobility of charge carries, PPy always acts as a stable photosensitizer to enhance the photoactivity of narrow bandgap semiconductors such as $TiO_2$.[9] As a p-type organic semiconductor, PPy is also used to prepare heterojunction displaying remarkable performance of light-controlled diode when combined with n-type semiconductors.[10] Furthermore, 1D nanotubes of conducting PPy can reversibly open and close by applying switch potentials in situ, which is analogous to biological nanochannels.[11] In spite of the outstanding optical property and interesting gating function, little endeavor has been devoted to create synthetic light-responsive nanochannels using PPy.

Here, for the first time, we integrate conductive PPy with alumina ($Al_2O_3$) nanopore arrays to obtain organic/inorganic

Dr. Q. Zhang, Prof. Z. Liu, Dr. K. Wang, Prof. J. Zhai
Key Laboratory of Bioinspired Smart Interfacial Science and Technology of Ministry of Education
Beijing Key Laboratory of Bioinspired Energy Materials and Devices
School of Chemistry and Environment
Beihang University
Beijing 100191, P.R. China
E-mail: liuzy@buaa.edu.cn; zhaijin@buaa.edu.cn

DOI: 10.1002/adfm.201404160

hybrid artificial nanochannels with pH- and light-modulated ion transport characteristics. The flexible structure of PPy polymer limits their direct application as nanochannels. Therefore, porous $Al_2O_3$ membrane consisting of nanopore arrays, which features robust mechanical strength, uniform pore distribution, and easy availability, is chosen as a template to fabricate PPy/$Al_2O_3$ hybrid nanochannels. To obtain asymmetric chemical component of nanochannels, conducting PPy is partially deposited on the interior surface of $Al_2O_3$ nanopores. The surface charge discontinuous distribution along nanochannels caused by the protonation/deprotonation of surface groups upon pH variation contributes to the pH-modulated ion rectification. The cooperative effect of light and protons induced positive charge generation on PPy segment, which can be used to regulate the ion flux through the nanochannels and results in a light-responsive ion current. Furthermore, the light-responsive ionic current could be enhanced by optimizing this cooperation. Our organic/inorganic hybrid stimuli-responsive nanochannels combine advantages of unique optical and electric properties from conducting PPy and high mechanical performance from porous $Al_2O_3$ membrane, demonstrating excellent stability, reversibility, and sensitivity.

## 2. Results and Discussion

### 2.1. Characterization Studies

As shown in **Scheme 1**, the fabrication of hybrid nanochannels consisted of two steps: 1) deposition of Au on one side of porous $Al_2O_3$ membrane by ion sputtering as a conductive layer; 2) electrochemical growth of PPy in $Al_2O_3$ nanochannels from the Au conductive layer. The obtained PPy/$Al_2O_3$ hybrid nanochannels demonstrate deep color and low transparency (Scheme 1). The morphology and pore size of hybrid nanochannels are characterized by the scanning electron microscope (SEM) images. It can be determined that the average pore diameter of $Al_2O_3$ porous membrane is 49 nm with a distribution from ≈44 to ≈55 nm (**Figure 1**A, Figure S1 and Figure S2A, Supporting Information). When sputtering a thin layer of Au as a conducting layer, the pore size of bottom side shrinks lightly for the cover of gold nanoparticles (Figure 1B). The thickness of $Al_2O_3$ membrane is estimated to be ≈73 μm from the cross-sectional image (Figure 1C). Two specified areas in the red solid and blue dashed boxes (as shown in Figure 1C) are chosen from cross-section to illustrate the asymmetric distribution of PPy along $Al_2O_3$ nanochannels. Straight nanochannels parallel to each other are clearly observed in the magnified cross-sectional images (Figure 1D,E). The channel diameter of the red solid part is ≈39 nm (Figure S3A, Supporting Information), which is slightly smaller than that of the blue dashed part (≈49 nm as shown in Figure S3B, Supporting Information) because of the growth of PPy along the channel wall from the conductive Au layer. Energy-dispersive X-microanalysis (EDX) was used to investigate the surface chemical elements of these two specific spots. As shown in Figure S4 (Supporting Information), the detected major elements are carbon and nitrogen in the red solid box, which are from the PPy layer in the nanochannels. Correspondingly, in the blue dashed box, the major elements are aluminum and oxygen. The thickness of PPy layer in the $Al_2O_3$ nanochannels is about 26 μm from the dispersion of carbon element in the element mapping (Figure S4, Supporting

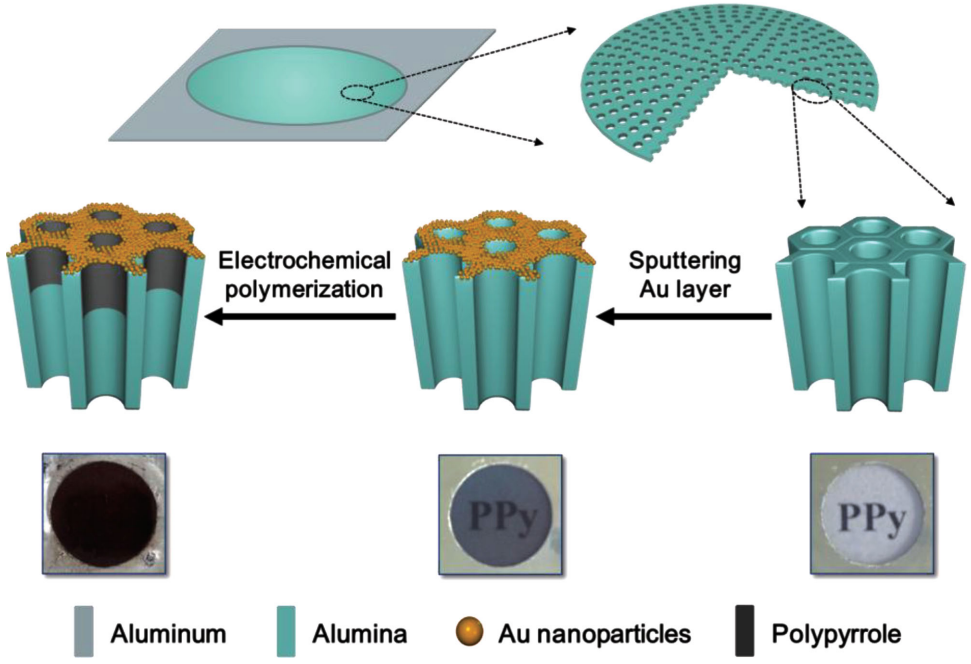


**Scheme 1.** Schematic illustration for the fabrication of PPy/$Al_2O_3$ hybrid nanochannels and photographs corresponding to each stages. The pristine $Al_2O_3$ porous membrane is transparent. Au nanoparticles are sputtered onto one side of porous $Al_2O_3$ membrane as a conductive layer. Polypyrrole is introduced into $Al_2O_3$ nanochannels from Au side by electrochemical polymerization. After PPy modification, the hybrid porous membrane demonstrates deep color and low transparency.

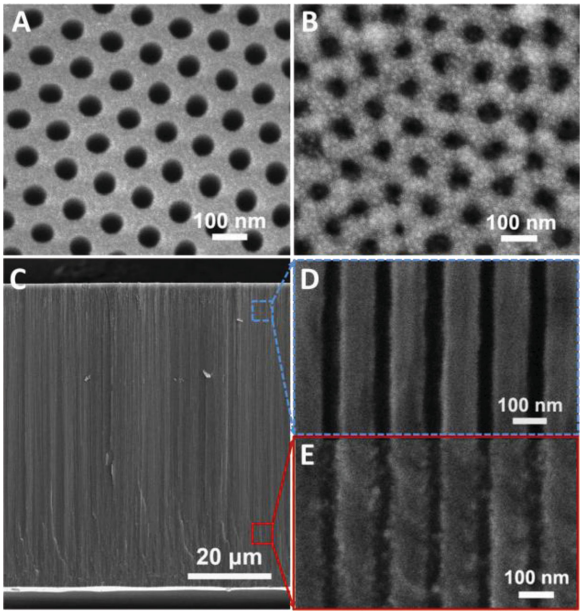


**Figure 1.** SEM images of PPy/$Al_2O_3$ hybrid nanochannels with mean diameter of ≈49 nm. A) top side; B) bottom side covered with Au nanoparticles; C) cross-section; D,E) magnified images of specific area. The pore diameter of $Al_2O_3$ porous membrane is ≈49 nm. The cover of Au nanoparticles shrinks the pore diameter to be ≈39 nm. PPy grows along $Al_2O_3$ nanochannels from the Au side, which fills $Al_2O_3$ nanochannels partially. The hybrid nanochannels exhibit an asymmetric chemical composition.

Information). These results indicate that PPy is partially modified on the inner surface of $Al_2O_3$ nanochannels.

Infrared (IR) spectroscopy was used to further clarify the existence of PPy embedded into the hybrid nanochannels. In comparison with pristine $Al_2O_3$ nanochannels, the IR spectrum of hybrid nanochannels displays several typical characteristic peaks of PPy (**Figure 2**A). The peaks at 1674 and 1608 $cm^{-1}$ belong to C=C stretching vibration and N–H bending vibration in the pyrrole ring, respectively.[12a] Two bands appearing at 1454 and 1392 $cm^{-1}$ are assigned to the =C–H bending vibration, and a band at around 1126 $cm^{-1}$ could be assigned to C–N stretching.[12b] The peaks observed at 876 and 783 $cm^{-1}$ are ascribed to the =C–H out of plane deformation vibration indicating polymerization of pyrrole.[12c] The UV–visible (UV) absorption spectra of the hybrid PPy/$Al_2O_3$ nanochannels and pristine $Al_2O_3$ nanochannels are illustrated in Figure 2B. The PPy/$Al_2O_3$ sample displays a typical absorption band of PPy at 481 that can be attributed to the characteristics of $\pi$–$\pi^*$ transition.[13] The weak shoulder appearing at 580 nm could be ascribed to electron transition from highest occupied molecular orbital (HOMO) of PPy to the lowest unoccupied molecular orbital (LUMO).[14] The significant increase of absorption intensity in the whole wavelength range can be observed when introducing PPy into the $Al_2O_3$ membrane, mainly because PPy has strong absorption ability in the UV and visible light range.

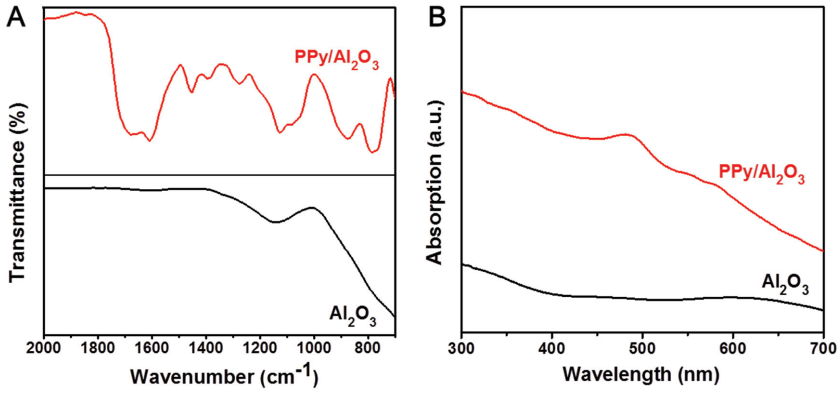


**Figure 2.** A) Micro-IR and B) UV–vis absorption spectra of PPy/$Al_2O_3$ hybrid and $Al_2O_3$ nanochannels.

### 2.2. Stimuli-Modulated Ion Transport

In hybrid nanochannels, the discontinuous distribution of surface charge including charge polarity and density could be regulated by changing the pH value of electrolyte, which subsequently influenced the ion transport through the nanochannels. The pH-modulated ionic transport property was characterized by measuring the current–voltage (*I–V*) curves under different pH values. The electrolyte was fixed to be $1 \times 10^{-3}$ M KCl aqueous solution and the anode was faced to PPy side of hybrid nanochannels during the test. When the pH value of electrolyte is determined to be 3.0, which is lower than the isoelectric point of alumina (≈8.5),[15] the inner surface of $Al_2O_3$ nanochannels without coverage of PPy is positively charged due to the protonation. Meanwhile, the surface of PPy with imino groups is estimated to carry positive charges because the p*Ka* of amino groups assembled on interface is 7.4.[16] Although the whole interior surface of nanochannels is positively charged, the charge density on PPy part owing high polymerization degree is much higher than that on the unmodified $Al_2O_3$ portion, which leads to an asymmetric distribution of charge density along the nanochannels (I state in **Figure 3**A). Furthermore, the average pore radius of hybrid nanochannels is comparable to the thickness of electric double layer (EDL) formed in $1 \times 10^{-3}$ M KCl electrolyte (≈9.8 nm). In this case, positively charged hybrid nanochannels incorporate counterions (mainly $Cl^-$) and exclude cations,[17] so $Cl^-$ ions preferentially transport through nanochannels from more positively charged side with PPy modification. As a result, the ionic current is higher when applied negative voltage (anode was faced to PPy side), which makes the hybrid nanochannels exhibit nonlinear *I–V* curves as shown in Figure 3B. At high pH value of 10.0, alumina surface is negatively charged while the imino groups of PPy are neutral (II state in Figure 3A). The partially negatively charged hybrid nanochannels demonstrate cations (mainly $K^+$) selectivity,[17] which rectify the ionic current as shown in Figure 3B. Furthermore, the *I–V* curves are reverse when the anode and cathode are switched, which indicates that the ion transport through hybrid nanochannels

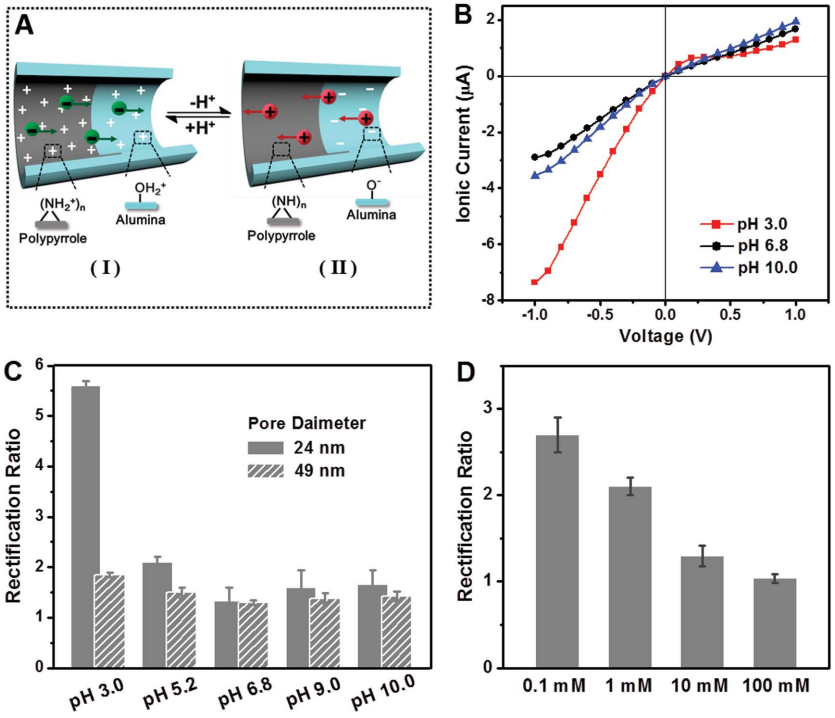


**Figure 3.** A) Illustration of surface charge and ion transport changes occurring in the hybrid nanochannels upon variations of pH value. At a low pH value (I state), the surface of $Al_2O_3$ and polypyrrole both carry positive charges. The high polymerization degree of PPy makes the charge density on PPy segment be much higher. At a high pH value (II state), $Al_2O_3$ is negatively charged, while PPy is neutral. B) Current–voltage (*I–V*) curves of PPy/$Al_2O_3$ hybrid nanochannels with diameter of ≈24 nm measured in $1 \times 10^{-3}$ M KCl with different pH values. The hybrid nanochannels display pH-responsive ion rectification characteristics. C) The calculated ionic current rectification ratios of hybrid nanochannels with different pore sizes under different pH conditions. The increase in pore size reduces the rectification ratio. D) Ionic current rectification ratios of hybrid nanochannels with diameter of ≈24 nm measured in KCl electrolyte with different concentrations under pH value of 5.2. The decrease in electrolyte concentration increases the rectification ratio.

is surface charge-governed (Figure S5, Supporting Information). Therefore, inhomogeneous distribution of surface charge along the hybrid nanochannels could be modulated in a broad range of pH, which contributes to pH-responsive ionic rectifying behavior. Based on five cycles of asymmetric *I–V* curves as shown in Figure S6 (Supporting Information), the ion rectification characteristic demonostrates good reversibility and stability.

Ionic current rectification ratio, as a quantitative factor describing ion rectification properties, was defined to be the ratio between the absolute values of the ionic current at −1 V and +1 V voltage in this system. The rectification ratio increases following the enhanced asymmetry of charge distribution along nanochannels. A low pH value promotes the protonation, especially for PPy, which makes the inhomogeneous distribution of positive charges become more obvious and thus benefits for raising the rectification ratio. As shown in Figure 3C, the rectification ratio measured in acidic solutions is larger than that recorded in alkaline solutions, which reaches its maximum value of ≈5.6 at pH 3.0 for hybrid nanochannels with diameter of ≈24 nm. When increasing the pore size of nanochannels to be ≈49 nm, *I–V* curves exhibit similar rectification behavior, but the rectification ratios are lower than that of the nanochannels with diameter of ≈24 nm under the same conditions (Figure 3C). That is because the EDL layer could not overlap the nanopore completely. In this case, the effect of surface-charge-governed ion transport through nanochannels is weakened, which is not benefit for ion rectification.[18] It is noteworthy that no ionic rectification characteristics were detected in blank $Al_2O_3$ nanochannels and $Al_2O_3$ nanochannels covered with Au conducting layer under any pH values (Figure S7, Supporting Information). Furthermore, the ionic current rectification ratio is sensitive to the concentration of electrolyte as shown in Figure 3D. For $0.1 \times 10^{-3}$ M KCl electrolyte, the ionic rectification behavior with the ratio of ≈2.7 is observed (Figure S8A, Supporting Information). Then, increasing the electrolyte concentration resulted in a loss of ionic rectification ratio. When the concentration of KCl electrolyte is $100 \times 10^{-3}$ M, no rectifying behavior displayed by the hybrid nanochannels could be found (Figure S8D, Supporting Information). The thickness of EDL decreases with an increase of electrolyte concentration.[19] In the condition of low concentration, the EDL thickness is much larger than the radius of nanochannels. In this case, the ion transport property is fully governed by the surface charge. So the asymmetric surface charge distribution along nanochannels contributes to obvious ion rectification. For a high concentration of electrolyte, the radius of hybrid nanochannels is much larger than the EDL thickness, which greatly weakens surface-charge-governed ion transport. Therefore, no obvious ion rectification characteristic could be observed.

In order to quantitatively explain the ion rectification mechanism in this nanochannel system, a theoretical model based on Poisson and Nernst-Plank (PNP) equations was established. For simplicity, our model was set as cylindrical single nanopore with symmetric structure but inhomogeneous surface charge distribution (as shown in Figure S9, Supporting Information). The surface charge density, polarity, and distribution along the nanopore varied with different pH values of solution. According to previous analysis, we set surface charge density of PPy segment as $s_1 = +10\ e\ nm^2$ and that of unmodified $Al_2O_3$ part as $s_2 = +1\ e\ nm^2$ for pH 3. For pH value of 6.8 and 10, the surface charge density was set as $s_1 = +0.5\ e\ nm^2$, $s_2 = +0.1\ e\ nm^2$, and $s_1 = 0\ e\ nm^2$, $s_2 = -1\ e\ nm^2$ respectively. Under the condition of pH 3, concentration of $Cl^-$ is larger than that of $K^+$ (Figure S10A,B, Supporting Information) since anions are majority carriers in a positively charged nanopore. When applying −1 V bias, the enrichment of ions (both $Cl^-$ and $K^+$) contributes to high ion concentration as shown in Figure S10A (Supporting Information). The nanopore exhibits high conductance, which produces large ionic current. However, applying

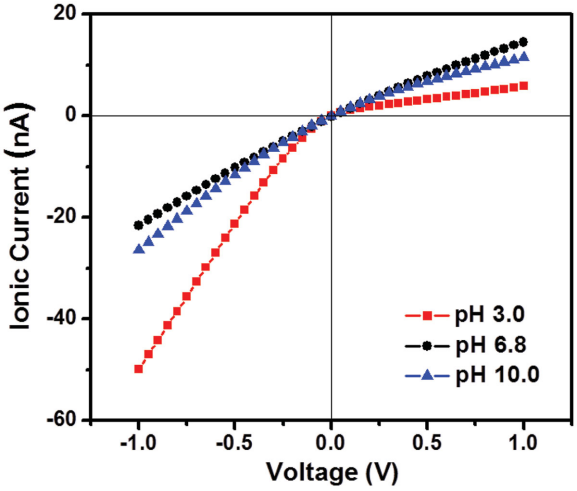


**Figure 4.** Simulated ion current–voltage (I–V) curves under different pH values based on the theoretical model. For pH 3, the surface charge density of PPy and $Al_2O_3$ segment is set as $s_1 = +10\ e\ nm^2$ and $s_2 = +1\ e\ nm^2$. For pH value of 6.8 and 10, the surface charge density are set as $s_1 = +0.5\ e\ nm^2$, $s_2 = +0.1\ e\ nm^2$ and $s_1 = 0\ e\ nm^2$, $s_2 = -1\ e\ nm^2$, respectively.

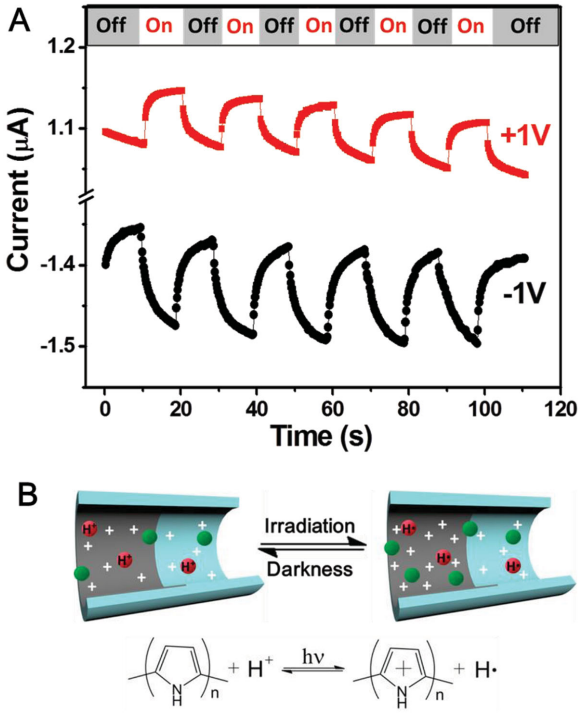


**Figure 5.** A) Ionic current–time traces of PPy/$Al_2O_3$ hybrid nanochannels (pore diameter = ≈24 nm) at +1 V and −1 V constant voltages when the incident light irradiance is in situ switched on (ON) and off (OFF). The increase in ionic current through hybrid nanochannels by light illumination indicates that the ion flux can be regulated by light. The measurement is carried out in $1 \times 10^{-3}$ M KCl electrolyte with pH value of 6.8. The light source is simulated full light with an irradiance of 98.5 mW $cm^{-2}$. B) Schematic diagram for the light-induced surface charge variations on PPy segment by the cooperative effect of light and protons (pH 6.8). The light-induced electrons in excited PPy are captured by protons in the electrolyte and the holes are left.

opposite bias (+1 V) results in the depletion of ion concentration, especially for $K^+$ (Figure S10B, Supporting Information), which subsequently decreases the ionic current. Therefore, the simulated *I–V* curve shows the nonlinear behavior (**Figure 4**), which is consistent with our experiment results. For pH value of 10, the situation of ion enrichment and depletion is similar to acidic condition because the charge polarity and distribution of nanopore are both reserved (Figure S10C,D, Supporting Information). However, the difference of ion concentration between two applied bias is smaller than that under pH 3, which reduces ion rectification ratio from the simulated *I–V* curve (Figure 4).

As multi-stimuli-responsive artificial nanochannels, except for pH-responsive characteristic, the hybrid nanochannels also exhibit light-regulated ion flux owing to the intrinsic optical properties of PPy. The incident light used in the test was simulated full light with an irradiance of 98.5 mW $cm^{-2}$, which was irradiated on the hybrid nanochannels as shown in Figure S11 (Supporting Information). Fluctuation of ionic current can be observed distinctly from the ionic current–time (*I–t*) trace curves measured using $1 \times 10^{-3}$ M KCl electrolyte (pH 6.8) at constant voltages of +1 V and −1 V when the incident light is in situ switched on and off alternately, as illustrated in **Figure 5**A. Here, we defined the light-responsive ionic current to be the difference between the maximum value of ionic current under light irradiation and that in the darkness, which results from the change of ion flux induced by light. At +1 V voltage, the ionic current increases immediately with responsive ionic current of ≈56 nA upon light irradiation, then it returns to its original value as soon as the incident light is shut down. When applied an opposite polarity of voltage (−1 V), the same responsive trend of the ionic current is observed with a fluctuating value of ≈118 nA. The fast generation of light-responsive ionic current endows the hybrid nanochannels with a sensitive light-regulated ion flux characteristic. Five cycles of light on–off illumination suggest that the hybrid nanochannels demonstrate excellent reversibility and stability. In contrast, no light response occurs on the ionic current recorded using $Al_2O_3$ nanochannels under the same testing conditions (Figure S12, Supporting Information), which indicates that PPy plays a crucial role on the light-responsive performance displayed by the hybrid nanochannels.

The generation of light-responsive ion current (i.e., the regulation of ion flux) can be attributed to the cooperative effect of light and protons, which increases the surface positive charge density in PPy segment upon light irradiation and subsequently increases the ionic conductivity in the hybrid nanochannels (Figure 5B). At pH 6.8, alumina and PPy are both considered to be positively charged. However, the high polymerization degree of PPy renders it to carry more positive charges. Under illumination, electrons are excited from the highest occupied molecular orbit (HOMO) of PPy to the lowest unoccupied molecular orbit (LUMO).[9b,20] The energy level of LUMO of PPy is located at −2.3 eV (vs NHE).[21] The hydrogen reduction potential (Φ) in pH 6.8 is determined to be −0.4 eV (vs NHE) based the Nernst equation of Φ (V vs NHE) = −0.059pH. Therefore, the light-induced electrons are possibly captured by protons in the electrolyte to form hydrogen radical (H·) and holes are left, which enhances the positive charge density of PPy layer on the hybrid

nanochannels (Figure 5B). As a result, the ionic conductivity in the hybrid nanochannels is increased, which improves the magnitude of ionic current.[22] Meanwhile, the enhanced asymmetry in charge distribution induced by light makes the absolute value of light-responsive ionic current at −1 V be larger than that at +1 V. The instable H· may recombine with holes in the PPy when the light is switched off, which contributes to the reversible light-responsiveness. The I–V curves of hybrid nanochannels under dark and light are shown in Figure S13 (Supporting Information). The incident light enhances the ionic current in the voltage range between −1 and +1 V. The variation value of ionic current (responsive current) at −1 V is larger than that at +1 V, which is accordance with the results of I–t trace measurements.

Based on above mechanism, the light-responsive ion current induced by the change of ion flux is supposed to be magnified by adjusting the proton content. From the I–t trace curves of hybrid nanochannels under light/dark switch (**Figure 6**A,B), it was found that the intensity of light-responsive current is dependent on the proton content in electrolyte proportionally. Besides, the responsive current value recorded at −1 V is larger than that at +1 V under each pH value (Figure 6C). As discussed above, the pH value of electrolyte will affect the surface charge distribution (I and II states in Figure 6D). In a low pH value, the high proton concentration decreases the potential of hydrogen reduction and favors the transfer of photogenerated electrons from excited PPy to the protons (middle inset in Figure 6D). More light-induced positive charges are formed in PPy segment, which maximizes the ionic conductivity, therefore results in a high-responsive ion current (II and III states in Figure 6D). When the pH value of electrolyte increases, the low proton concentration induces fewer positive charges in PPy segment (I and IV states in Figure 6D), which induces a small responsive ion current. Therefore, the responsive ionic current (i.e., the change of ion flux), especially for that recorded at −1 V voltage, could be greatly increased by the cooperation of light and pH stimulus.

The reversible and stable responsive properties of hybrid nanochannels upon alternating pH and light on–off illumination are illustrated in **Figure 7**. Compared with pristine $Al_2O_3$ nanochannels, the ionic current rectification ratio of hybrid nanochannels can be adjusted by changing the pH value of electrolyte between acidity (pH 3) and alkalinity (pH 10), which reflects the repeatability of pH-responsive ionic

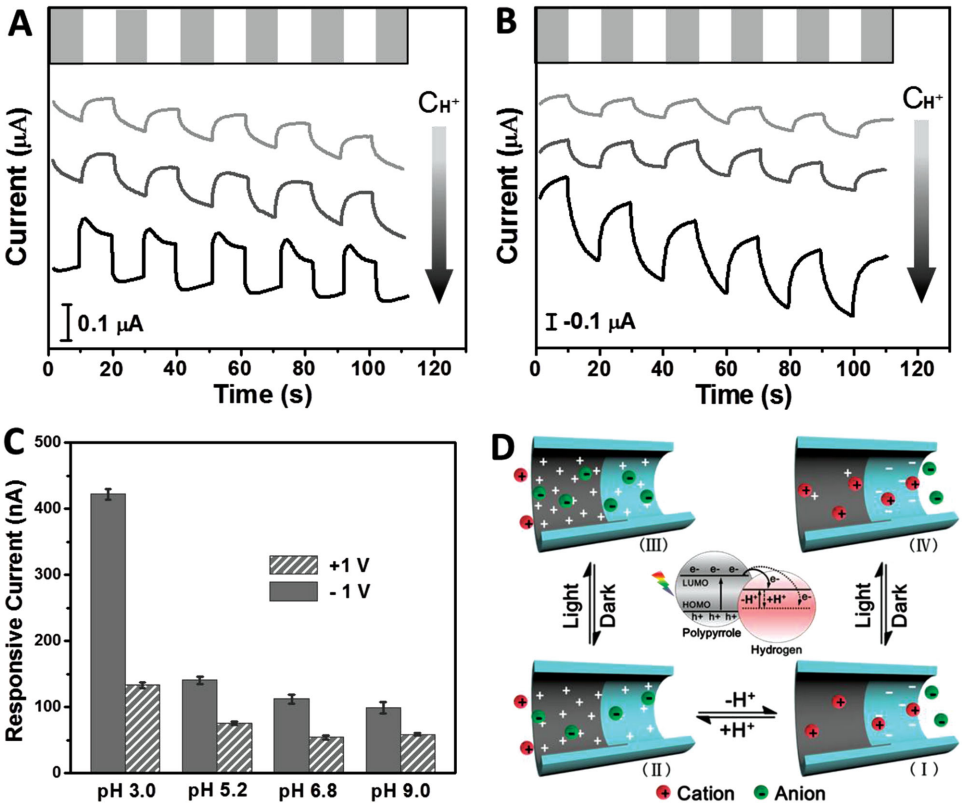


**Figure 6.** A,B) I–t curves of hybrid nanochannels (pore diameter = ≈24 nm) recorded at A) +1 V and B) −1 V voltage in $1 \times 10^{-3}$ M KCl electrolyte with various proton concentrations when light illumination is switched on and off. The increase in proton concentration enhances the light-responsive ion current at +1 and −1 V. C) The calculated light-responsive ionic currents through PPy/$Al_2O_3$ hybrid nanochannels at +1 V and −1 V voltages in $1 \times 10^{-3}$ M KCl electrolyte under different pH values. The light-responsive ion current is enhanced by the proton concentration. D) Schematic diagram for the effect of proton concentration on the light-induced surface charge variations on PPy segment. Inset: Capture of photogenerated electrons in excited PPy by protons in electrolyte. A low pH value lowers the hydrogen reduction potential. The surface charge distribution of hybrid nanochannels depends on the pH value of electrolyte (I and II states). A low pH value introduces more light-induced positive charges in PPy segment under illumination (II and III states) because of the lower hydrogen reduction potential when compared with a high pH value (I and IV states).

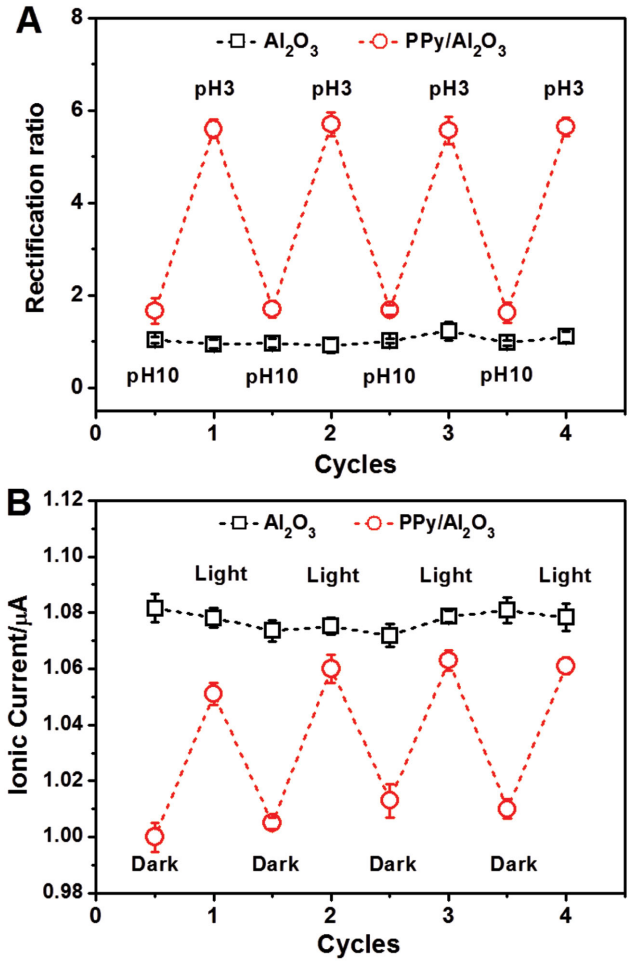


**Figure 7.** A,B) Reversible and stable switching ability of the hybrid PPy/$Al_2O_3$ and $Al_2O_3$ nanochannels for variation of A) pH values and B) light. The ionic current rectification ratio and ion flux of hybrid nanochannels can be adjusted by pH value and light, respectively. The electrolyte used in both test was $1 \times 10^{-3}$ M KCl aqueous solution. The light-responsive properties were recorded at +1 V voltage under pH value of 6.8. The pore diameter of nanochannels was ≈24 nm.

rectification (Figure 7A). Likewise, the cycles of variation on ionic current through hybrid nanochannels demonstrates the reproducible character of light-regulated ion flux (Figure 7B). In addition, each cycle could achieve in a short time. Especially for light response, the ionic current only needs a few seconds to reach stable upon light illumination (Figure 5A), which indicates that the hybrid nanochannels is fairly sensitive to external stimuli.

## 3. Conclusion

In summary, we demonstrate the integration of PPy conductive polymer into $Al_2O_3$ nanopore arrays to form stimulus-responsive organic/inorganic hybrid nanochannels displaying pH- and light-modulated ion transport characteristics. The asymmetric distribution of surface charges along the nanochannels under a broad range of pH values contributes to ion rectification, which is affected substantially by the pH value and the pore size of nanochannels. The regulation of ion flux can be ascribed to the introduction of positive charges in PPy segment by the cooperative effect of light and protons, which increases the ionic conductivity. The stability, reversibility, and sensitivity make PPy/$Al_2O_3$ hybrid nanochannels be a platform for creating smart nanochannels system.

## 4. Experimental Section

*Nanochannels Preparation*: The fabrication of PPy/$Al_2O_3$ hybrid nanochannels is outlined as shown in Figure 1A. $Al_2O_3$ porous membranes (AAO, Puyuan Nano, China) containing straight nanochannels with mean pore diameter of ≈24 nm and ≈49 nm were used as templates in this work. First, a layer of Au nanoparticals was sputtered on one side of $Al_2O_3$ membrane ($\phi = 12$ mm) as a conducting layer. The deposition of PPy in $Al_2O_3$ porous membrane was achieved by electrochemical polymerization of pyrrole using galvanostatic methods with a current density of 0.9 mA $cm^{-2}$.[11,23] The current for polymerization was provided by a CHI660D electrochemical workstation (Shanghai Chenhua Apparatus Co., China). Au-sputtered $Al_2O_3$ membrane was used as a working electrode and a platinum sheet acted as a counter electrode. The reference electrode is saturated calomel electrode (SCE). The electrolyte was phosphate buffer solution (PBS, 0.5 mol $L^{-1}$, pH 6.8) containing 0.2 mol $L^{-1}$ pyrrole (Py, J&K Scientific Ltd., China) and 0.01 mol $L^{-1}$ $\beta$-naphthalenesulfonic acid (NSA, Tokyo Kasei Kogyo Co. Ltd., Japan). By controlling the electrochemical polymerization time, PPy was partially deposited on the inner surface of nanopores in $Al_2O_3$ membrane. Finally, the obtained hybrid membrane was cleaned by deionized water for latter measurements.

*Characterization*: The morphologies of PPy/$Al_2O_3$ hybrid nanochannels were observed by a FEI Quanta FEG 250 environmental SEM and a JEOL JSM-7500F field-emission scanning electron microscope (FESEM). An INCA Energy 250 energy spectrum analyzer was used to detect the surface chemical elements of cross-section. Micro-IR spectrum was measured using a Nicolet iN10MX Micro-infrared spectrometer. UV–vis absorption spectrum was recorded with a Shimadzu UV-3600 ultraviolet visible near-infrared spectrometer.

*Ion Current Measurements*: The ion transport properties of PPy/$Al_2O_3$ hybrid nanochannels were studied by measuring the current–voltage (I–V) and current–time (I–t) behaviors. During the measurement, the nanochannels were mounted between two chambers of double-chamber electrochemical cell with a quartz window. KCl (Beijing Chemical Factory) aqueous solution with different pH values and concentrations were chosen as a electrolyte. The pH value of electrolyte was adjusted using 1 mol $L^{-1}$ HCl and KOH solutions. Two Ag/AgCl electrodes were used to apply a transmembrane potential across the hybrid nanochannels. The PPy side of nanochannels was defined to be the positive potential. Ion current was measured by a Keithley 6487 picoammeter (Keithley Instruments, Cleveland, OH). The light source was provided by an Xe lamp (Beijing Perfectlight Technology Co. Ltd, China) with an irradiance of 98.5 mW $cm^{-2}$ measured with a power meter (UV-A, Photoelectric Instrument Factory of Beijing Normal University). The transmembrane voltage varied from −1 V to +1 V with a 40 s period during the I–V property measurements. The constant voltages of +1 V and −1 V were applied for measuring I–t traces. Each test was repeated four times to obtained average ionic current values. The testing temperature was the room temperature. For control experiment, ion transport characteristics of blank $Al_2O_3$ nanochannels and $Al_2O_3$ nanochannels covered with Au conductive layer were also investigated.

## Supporting Information

Supporting Information is available from the Wiley Online Library or from the author.

## Acknowledgements

This work was supported by the National Basic Research Program of China (2011CB935704), National Natural Science Foundation of China (21003008, 21073009), Beijing Natural Science Foundation (2133066), "Young Talents Plan" for the Universities in Beijing City, Innovation Foundation of BUAA for PhD Graduates (YWF-14-YJSY-046), Fundamental Research Funds for the Central Universities (YWF-14-HHXY-004). The authors thank Dr. Zheyi Meng for building the model.

Received: November 24, 2014
Revised: January 16, 2015
Published online: February 6, 2015

[1] a) B. Hille, *Ion Channels of Excitable Membranes*, Sinauer Associates, Sunderland, MA **2001**; b) E. Gouaux, R. MacKinnon, *Science* **2005**, *310*, 1461; c) C. Dekker, *Nat. Nanotechnol.* **2007**, *2*, 209; d) Z. S. Siwy, S. Howorka, *Chem. Soc. Rev.* **2010**, *39*, 1115; e) X. Hou, W. Guo, L. Jiang, *Chem. Soc. Rev.* **2011**, *40*, 2385; e) W. Guo, Y. Tian, L. Jiang, *Acc. Chem. Res.* **2013**, *46*, 2834.

[2] a) G. Wang, B. Zhang, J. R. Wayment, J. M. Harris, H. S. White, *J. Am. Chem. Soc.* **2006**, *128*, 7679; b) B. Yameen, M. Ali, R. Neumann, W. Ensinger, W. Knoll, O. Azzaroni, *Small* **2009**, *5*, 1287; c) B. Yameen, M. Ali, R. Neumann, W. Ensinger, W. Knoll, O. Azzaroni, *Nano Lett.* **2009**, *9*, 2788; d) Y. Zhou, W. Guo, J. Cheng, Y. Liu, J. Li, L. Jiang, *Adv. Mater.* **2012**, *24*, 962; e) Z. S. Siwy, M. R. Powell, A. Petrov, E. Kalman, C. Trautmann, R. S. Eisenberg, *Nano Lett.* **2006**, *6*, 1729; f) M. R. Powell, M. Sullivan, I. Vlassiouk, D. Constantin, O. Sudre, C. C. Martens, R. S. Eisenberg, Z. S. Siwy, *Nat. Nanotechnol.* **2008**, *3*, 51; g) M. Ali, S. Nasir, P. Ramirez, J. Cervera, S. Mafe, W. Ensinger, *ACS Nano* **2012**, *6*, 9247; h) G. Wang, A. K. Bohaty, I. Zharov, H. S. White, *J. Am. Chem. Soc.* **2006**, *128*, 13553; i) M. Ali, S. Nasir, P. Ramirez, I. Ahmed, Q. H. Nguyen, L. Fruk, S. Mafe, W. Ensinger, *Adv. Funct. Mater.* **2012**, *22*, 390; j) Q. Zhang, Z. Liu, X. Hou, X. Fan, J. Zhai, L. Jiang, *Chem. Commun.* **2012**, *48*, 5901; k) Z. S. Siwy, L. Trofin, P. Kohli, L. A. Baker, C. Trautmann, C. R. Martin, *J. Am. Chem. Soc.* **2005**, *127*, 5000.

[3] a) M. Ali, B. Yameen, R. Neumann, W. Ensinger, W. Knoll, O. Azzaroni, *J. Am. Chem. Soc.* **2008**, *130*, 16351; b) I. Vlassiouk, T. R. Kozel, Z. S. Siwy, *J. Am. Chem. Soc.* **2009**, *131*, 8211; c) L. Wen, X. Hou, Y. Tian, F. Nie, Y. Song, J. Zhai, L. Jiang, *Adv. Mater.* **2010**, *22*, 1021; d) M. Ali, M. N. Tahir, Z. S. Siwy, R. Neumann, W. Tremel, W. Ensinger, *Anal. Chem.* **2011**, *83*, 1673; e) R. Wei, V. Gatterdam, R. Wieneke, R. Tampe, U. Rant, *Nat. Nanotechnol.* **2012**, *7*, 257; f) R. Duan, F. Xia, L. Jiang, *ACS Nano* **2013**, *7*, 8344.

[4] a) C. Geismann, F. Tomicki, M. Ulbricht, *Sep. Sci. Technol.* **2009**, *44*, 3312; b) A. Friebe, M. Ulbricht, *Macromolecules* **2009**, *42*, 1838; c) X. Hou, F. Yang, L. Li, Y. Song, L. Jiang, D. Zhu, *J. Am. Chem. Soc.* **2010**, *132*, 11736; d) W. Guo, H. Xia, L. Cao, F. Xia, S. Wang, G. Zhang, Y. Song, Y. Wang, L. Jiang, D. Zhu, *Adv. Funct. Mater.* **2010**, *20*, 3561; e) L. Zhang, S. Cai, Y. Zheng, X. Cao, Y. Li, *Adv. Funct. Mater.* **2011**, *21*, 2103.

[5] a) M. Zhang, X. Hou, J. Wang, Y. Tian, X. Fan, J. Zhai, L Jiang, *Adv. Mater.* **2012**, *24*, 2424; b) L. Wen, Q. Liu, J. Ma, Y. Tian, C. Li, Z. Bo, L. Jiang, *Adv. Mater.* **2012**, *24*, 6193; c) K. Xiao, G. Xie, P. Li, Q. Liu, G. Hou, Z. Zhang, J. Ma, Y. Tian, L. Wen, L. Jiang, *Adv. Mater.* **2014**, *26*, 6560.

[6] S. F. Buchsbaum, G. Nguyen, S. Howorka, Z. S. Siwy, *J. Am. Chem. Soc.* **2014**, *136*, 9902.

[7] a) P. Y. Apel, Y. E. Korchev, Z. S. Siwy, R. Spohr, M. Yoshida, *Nucl. Instrum. Methods Phys. Res. B* **2001**, *184*, 337; b) C. C. Harrell, Z. S. Siwy, C. R. Martin, *Small* **2006**, *2*, 194.

[8] a) F. S. Kim, G. Ren, S. A. Jenekhe, *Chem. Mater.* **2011**, *23*, 682; b) M. Chen, X. Fang, S. Tang, N. Zheng, *Chem. Commun.* **2012**, *48*, 8934; c) Z. Yin, Q. Zheng, *Adv. Energy Mater.* **2012**, *2*, 179; d) K. Wang, H. Wu, Y. Meng, Z. Wei, *Small* **2014**, *10*, 14.

[9] a) N. M. Dimitrijevic, S. Tepavcevic, Y. Liu, T. Rajh, S. C. Silver, D. M. Tiede, *J. Phys. Chem. C* **2013**, *117*, 15540; b) Y. Yang, J. Wen, J. Wei, R. Xiong, J. Shi, C. Pan, *ACS Appl. Mater. Interfaces* **2013**, *5*, 6201; c) F. Deng, L. Min, X. Luo, S. Wu, S. Luo, *Nanoscale* **2013**, *5*, 8703.

[10] a) Y , Guo, Q. Tang, H. Liu, Y. Zhang, Y. Li, W. Hu, S. Wang, D. Zhu, *J. Am. Chem. Soc.* **2008**, *130*, 9198; b) Y. Guo, Y. Zhang, H. Liu, S. Lai, Y. Li, Y. Li, W. Hu, S. Wang, C. Che, D. Zhu, *J. Phys. Chem. Lett.* **2010**, *1*, 327.

[11] J. Liao, S. Huang, C. Ning, G. Tan, H. Pan, Y. Zhang, *RSC Adv.* **2013**, *3*, 14946.

[12] a) S. S. Barkade, D. V. Pinjari, A. K. Singh, P. R. Gogate, J. B. Naik, S. H. M. Ashokkumar, A. B. Pandit, *Ind. Eng. Chem. Res.* **2013**, *52*, 7704; b) D. Zhang, L. Luo, Q. Liao, H. Wang, H. Fu, J. Yao, *J. Phys. Chem. C* **2011**, *115*, 2360; c) T. Jiang, Z. Wang, Z. Li, W. Wang, X. Xu, X. Liu, J. Wang, C. Wang, *J. Mater. Chem. C* **2013**, *1*, 3017.

[13] N. M. Dimitrijevic, S. Tepavcevic, Y. Liu, T. Rajh, S. C. Silver, D. M. Tiede, *J. Phys. Chem. C* **2013**, *117*, 15540.

[14] a) H. Goto, *Polymers* **2011**, *3*, 875; b) G. Ge, J. He, H. Guo, F. Wang, D. Zou, *J. Organomet. Chem.* **2009**, *694*, 19, 3050.

[15] M. Kosmulski, *J. Colloid. Interface Sci.* **2004**, *275*, 214.

[16] H. Zhang, H. He, J. Wang, T. Mu, Z. Liu, *Appl. Phys. A*, **1998**, *66*, S269.

[17] a) Z. S. Siwy, E. Heins, C. C. Harrell, P. Kohli, C. R. Martin, *J. Am. Chem. Soc.* **2004**, *126*, 10850; b) H. S. White, A. Bund, *Langmuir* **2008**, *24*, 2212; c) C. Li, F. Ma, Z. Wu, H. Gao, W. Shao, K. Wang, X. Xia, *Adv. Funct. Mater.* **2013**, *23*, 3836.

[18] W. Chen, Z. Wu, X. Xia, J. Xu, H. Chen, *Angew. Chem. Int. Ed.* **2010**, *49*, 7943.

[19] a) K. Bohinc, V. Kralj-Iglič, A. Iglič, *Electrochim. Acta* **2001**, *46*, 3033; b) Q. Zhang, Z. Hu, Z. Liu, J. Zhai, L. Jiang, *Adv. Funct. Mater.* **2014**, *24*, 424.

[20] D. Wang, Y. Wang, X. Li, Q. Luo, J. An, J. Yue, *Catal. Commun.* **2008**, *9*, 1162.

[21] Y. Hao, M. Yang, W. L, X. Qiao, L. Zhang, S. Cai, *Sol. Energy Mater. Sol. Cells* **2000**, *60*, 349.

[22] a) D. Woermann, *Phys. Chem. Chem. Phys.* **2003**, *5*, 1853; b) J. Liu, M. Kvetny, J. Feng, D. Wang, B. Wu, W. Brown, G. Wang, *Langmuir* **2012**, *28*, 1588; c) Z. Meng, H. Bao, J. Wang, C. Jiang, M. Zhang, J. Zhai, L. Jiang, *Adv. Mater.* **2014**, *26*, 2329.

[23] J. Liao, Y. Zhang, G. Tan, C. Ning, *Surf. Coat. Technol.* **2013**, *228*, S41.